Physics of the Solid State, 2022, Vol. 64, No. 2

04,05

Crystal chemistry and magnetic properties of $BaFe_{12}O_{19}$ hexaferrite upon heterovalent substitution of iron with zirconium

© V.G. Kostishin[1], V.V. Korovushkin[1], I.M. Isaev[1], D.V. Salogub[1], S.V. Trukhanov[2], A.V. Trukhanov[1,2]

[1] National University of Science and Technology „MISiS“, Moscow, Russia
[2] Scientific and Practical Materials Research Center, National Academy of Sciences of Belarus, Minsk, Belarus

E-mail: truhanov86@mail.ru

Received October 20, 2021
Revised October 20, 2021
Accepted October 21, 2021

Samples of BaFe12O19 M-type barium hexaferrite with partial iron substitution by zirconium ions (concentration up to 10 at.%) have been synthesized and investigated. Studies of crystal features, phase composition, and magnetic properties were carried out using X-ray diffraction, Messbauer spectroscopy, and VSM respectively. The presence of limited heterovalent isomorphism by the $2Fe^{3+} \rightarrow Zr^{4+} + Fe^{2+}$ mechanism was shown. The limit of heterovalent isomorphic substitution by zirconium ions in barium hexaferrite ($x = 0.6$) was established. It was noted that additional sextets in the Messbauer spectra of barium hexaferrite can be formed during the localization of Zr^{4+} ions predominantly in the $12k$ and $4f_2$ positions due to the frustration of the magnetic structure. The correlation between the chemical composition (concentration of zirconium ions), impurity phase formation, the peculiarities of the distribution of substituents over oxygen coordination, and the magnetic properties was established.

Keywords: M-type barium hexaferrite, heterovalent substitution, limited isomorphism, Messbauer spectroscopy, magnetic properties

DOI: 10.21883/PSS.2022.02.52964.225

1. Introduction

Transition metal ion complex oxides attract the attention of researchers due to their combination of optimum magnetic and electric properties, as well as due to their chemical stability and corrosion resistance [1–3]. Hexagonal ferrites with magnetoplumbite structure (M-type) are one of the most actively studied and widely used in practice complex oxides of ferrous ions [4–8]. Changing the chemical composition of hexaferrites is an effective method to attain required magnetic, electric, and physical properties [9–11] and their use to improve performance of devices of magnetoelectronics [12], radioelectronics and SHF-electronics [13]. This can be explained by their wide isomorphic content and variety of isomorphic elements that can vary in a wide range. In most cases in this context isovalent substitution of ferrous ions by ions of metal with a close ion radius and an oxidation rate of 3+ is used because it allows quite easy implementation of charge balance (keeping the law of electroneutrality) [14,15]. At the same time the substitution of Fe^{3+} ions in the structure of hexaferrites by such ions as Al^{3+}, Sc^{3+} are used to increase coercitive force and, thus, magnetic hardness, which affects the quality of permanent magnets, allows the devices to work in strong magnetic fields and use their multiferroic properties [12,16]. The use of Ga^{3+}, In^{3+} isomorphic elements and some other elements on the contrary provides soft magnetic properties of ferrites, that are used in magnetic conductors working in magnetic fields of up to 100 MHz in pulse mode, in magnetic amplifiers, cores of transformers, inductors, and other devices [17,18]. An unusual behavior is demonstrated by the La^{3+} isomorphic element, where saturation magnetization increases with increase in x up to 0.1, while the magnetic hardness is increased as well and then it is decreased with further increase in x [19]. Doping hexaferrite with copper decreases both the saturation magnetization and the coercitive force [20].

In the case of heterovalent substitution of Fe^{3+} ions by M^{4+} or M^{2+} ions the charge balance can be implemented by several options. In the case of M^{4+} isomorphic elements an ion of M^{2+} can be added by the following scheme $2Fe^{3+} \rightarrow Me^{4+} + Me^{2+}$, for example, $Ti^{4+} + Co^{2+}$ [21] and vice versa, zinc and niobium [22], magnesium and zirconium [23], as well as by the following scheme $Fe^{3+} \rightarrow Fe^{2+} + Li^{+}$. In addition, electroneutrality in the case of doping with M^{4+} elements can be provided by recovery of the ferrum fraction to Fe^{2+} with partial electron exchange $Fe^{3+} \leftrightarrow Fe^{2+}$ [24],and in the case of doping with M^{2+} ions it can be accompanied by partial ferrum oxidation to the state of Fe^{4+} [25], as well as charge compensation due to cation vacancies for M^{4+} isomorphic elements, as in maghemite. All types of substitution result in a frustration of the magnetic structure and weakening of the exchange interactions (due-to the decrease in number of Fe−O−Fe bonds).

In this respect, the purpose of this work is to determine cation distribution in the $BaZr_xFe_{12-x}O_{19}$ (BaM-Zr) hexaferrite, to determine the limit of isomorphism, the mechanism of charge compensation, and the impact of isomorphic zirconium on its magnetic properties.

2. Research targets and methods

Target of the study were specimens of polycrystalline barium hexaferrite: $BaZr_xFe_{12-x}O_{19}$ or BaM-Zr, where $x = 0.1$; 0.3; 0.6; 0.9; 1.2. The specimens were produced using ceramic technology from Fe_2O_3, ZrO_2 oxides and $BaCO_3$ carbonate of „ultra high purity" grade. The preliminary initial compound was subjected to synthesizing annealing in the air at 1200°C (6 h), and then baked at 1300°C (6 h). After baking the specimens were slowly cooled in oven ($\sim$ 100°/h) [26]. Messbauer spectra of BaM-Zr specimens were recorded by Ms-1104 Em constant acceleration spectrometer, γ-radiation was sourced from Co^{57} in chromium matrix. Messbauer spectra were recorded at room temperature. The isomer (chemical) shift was calculated relative to α-Fe. Powder samples from baked ferrites were used, being fine-cut to 0.05–0.07 mm. The spectra were processed by „Univem Ms" program that demonstrates the best convergence between the experimental spectrum and the model of expansion with respect to $\min\chi^2$ parameter. Magnetic parameters: specific magnetization σs, residual magnetization σr, coercitive force H_c, field dependencies were measured by VSM 250 vibrating magnetometer in magnetic field with a strength of up to 20 kOe at room temperature. The synthesized specimens were studied for the composition of phases by the method of X-ray diffraction using diffractometer at 300 K (CuK_α radiation, $\lambda = 1.54$ Å) operated in the diffraction angle range 2θ from 20 to 80°.

3. Results and discussion

The analysis of phase composition of the synthesized hexaferrites for their single-phase condition and for the possibility of incomplete entering of Zr^{4+} ions into the hexaferrite lattice (Fig. 1) has shown that we can be assured that starting from $x = 0.6$ the zirconium is not completely included into the lattice and partially remains in the form of ZrO_2, and at $x = 0, 3$ it is difficult to detect it. With increase in zirconium content the content of phase increases, but not significantly. It can be assumed that the content of $x = 0.6$ is the limit of isomorphic entering of zirconium into the hexaferrite lattice. Note that the crystalline structure of the main phase for all BaM-Zr specimens can be described by a structure of magnetoplumbite type with the spatial group $P6_3/mmc$. The unit cell is composed of two formula units ($Z = 2$). It should be noted that with growth of the degree of substitution by zirconium ions the positions of diffraction peaks shift to the range of lower angles, which is the evidence of increase in the interplanar spacing and,

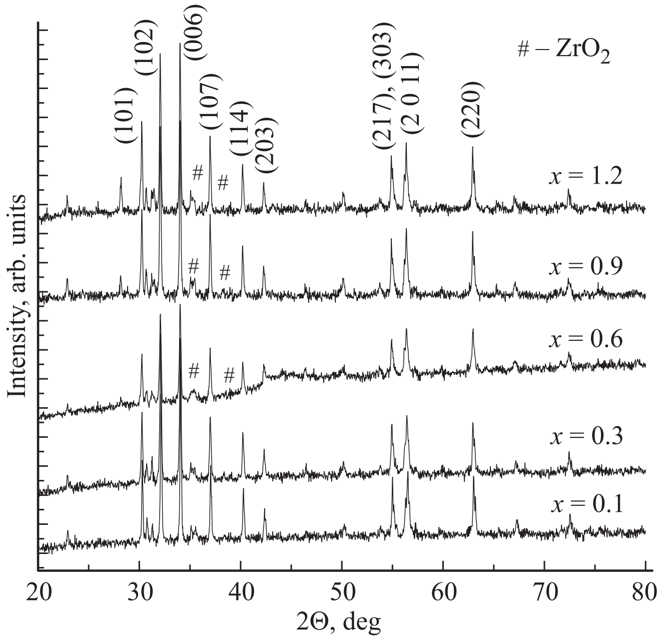

Figure 1. X-ray diffraction spectra of BaM-Zr specimens.

as a consequence, increase in parameters of the unit cell. It can be explained by the impact of the bigger ion radius of zirconium as compared with that of iron for all coordination numbers (CN): $r^{4+}_{\mathrm{Zr}} = 0.59$ Å and $r^{3+}_{\mathrm{Fe}} = 0.49$ Å (CN = 4); $r^{4+}_{\mathrm{Zr}} = 0.66$ Å and $r^{3+}_{\mathrm{Fe}} = 0.58$ Å (CN = 4) and $r^{4+}_{\mathrm{Zr}} = 0.72$ Å and $r^{3+}_{\mathrm{Fe}} = 0.64$ Å (CN = 4).

Messbauer spectra of BaM-Zr polycrystalline barium hexaferrites with a composition with (x) 0.1, 0.3, 0.6, 0.9, and 1.2 are illustrated in Fig. 2, and their Messbauer parameters are listed in the table: isomer (chemical) shift δ (mm/s), quadrupolar splitting Δ (mm/s), magnetic field on Fe^{57} nuclei (kOe), width of resonance line Γ (mm/s) and area of sextets (% rel.). To compare spectral parameters of substituted and non-substituted hexaferrites, Fig. 2, *a* shows Messbauer spectrum for non-substituted hexaferrite, and the table includes parameters for five positions of ions Fe: $12k$, $4f_1$, $4f_2$, $2a$, and $2b$.

All Messbauer spectra of substituted BaM-Zr hexaferrites have little visual difference from the initial spectrum, and the difference can only be noted by comparing the parameters obtained after processing by „Univem Ms" program. The results of this processing have shown that the best option is breaking down of all specimen spectra into 7 sextets.

It can be seen from the table that the biggest changes in the listed parameters are associated with integral intensities of the sextets related to entering of Zr^{4+} ions into the hexaferrite lattice, further redistribution of cations and the impact of this process on all parameters. In this regard, it is of interest to consider the dynamics of changes in the integral intensities depending on the degree of substitution x, shown in Fig. 3.

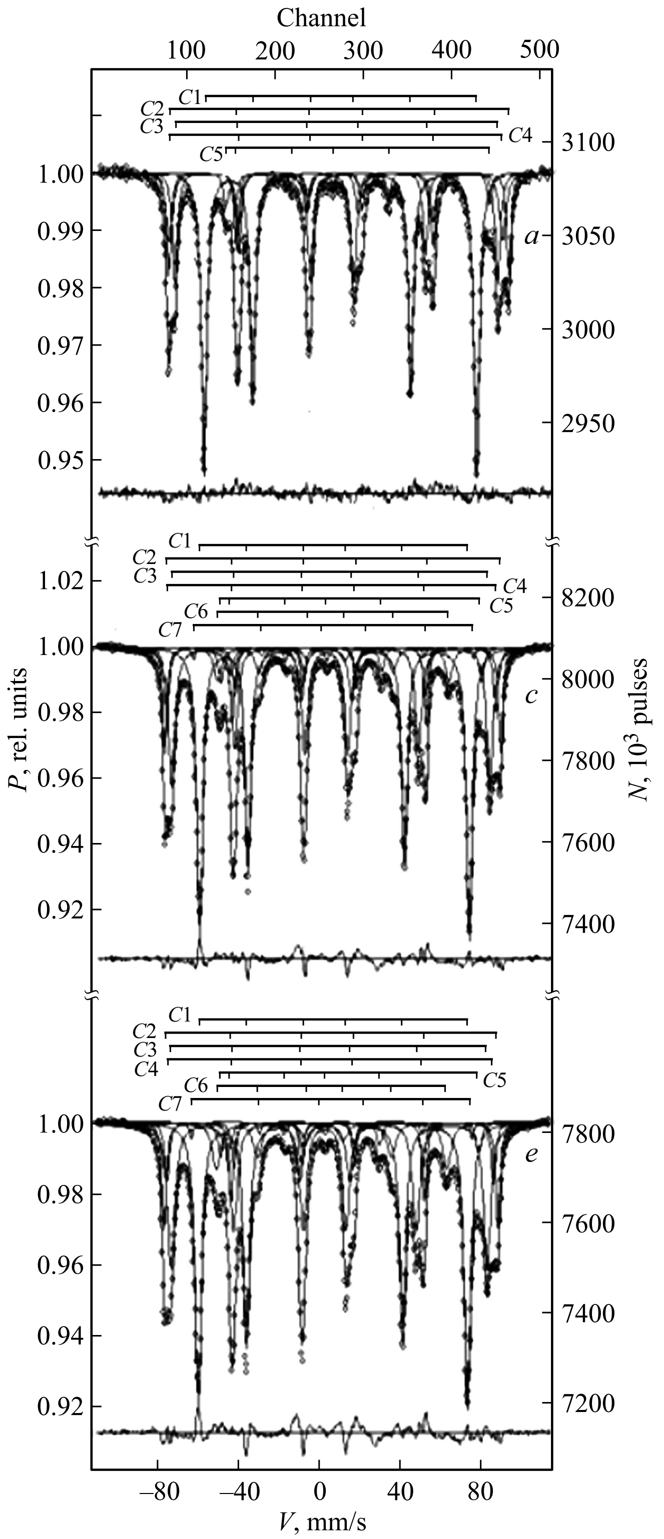

Figure 2. Messbauer spectra of BaM-Zr hexaferrite specimens at substitution values of x: a — 0.0, b — 0.1, c — 0.3, d — 0.6, e — 0.9, f — 1.2.

As can be seen from the changes in integral intensities (Fig. 3), generally they are not as significant as in the case of substitutions in $BaFe_{12-x}Me_xO_{19}$ hexaferrites with Ti^{4+}, In^{3+}, Sc^{3+}, Zn^{2+} at the same concentrations in the position of $12k$, where there are the biggest substitutions (see the table). At the same time, in the BaM-Zr hexaferrite integral intensities of Fe^{3+} $(12k)$ with $x = 1.2$ turned out to be lower (% rel.) by 12.5% as compared with substitutions

Parameters of Messbauer spectra of the Fe^{57} hexaferrite $BaFe_{12-x}Zr_xO_{19}$

Specimen of $BaFe_{12-x}Zr_xO_{19}$	Spectrum component	Isomer shift δ, mm/s	Quadrupolar splitting Δ, mm/s	Magnetic fields H_{eff}, kOe	Areas of components S, %	Line width Γ, mm/s
$x = 0.0$	$C1(12k)$	0.35	0.42	414	50.5	0.32
	$C2(4f_2)$	0.38	0.20	516	16.8	0.29
	$C3(4f_1)$	0.26	0.22	489	19.8	0.31
	$C4(2a)$	0.34	0.01	507	7.5	0.26
	$C5(2b)$	0.28	2.21	400	5.3	0.30
$x = 0.1$	$C1(12k)$	0.36	0.41	412	47.0	0.31
	$C2(4f_2)$	0.38	0.19	515	14.8	0.24
	$C3(4f_1)$	0.27	0.21	488	20.4	0.29
	$C4(2a)$	0.36	0.04	505	8.7	0.27
	$C5(2b)$	0.28	2.21	400	5.0	0.25
	$C6(12k^1)$	0.32	0.29	358	3.4	0.53
	$C7(4f_2^1)$	0.77	−0.47	427	0.7	0.21
$x = 0.3$	$C1(12k)$	0.36	0.41	412	44.5	0.35
	$C2(4f_2)$	0.39	0.18	513	11.5	0.24
	$C3(4f_1)$	0.27	0.21	486	23.6	0.38
	$C4(2a)$	0.38	0.08	502	8.1	0.28
	$C5(2b)$	0.28	2.20	397	4.5	0.30
	$C6(12k^1)$	0.33	0.36	353	6.6	0.44
	$C7(4f_2^1)$	0.74	−0.46	428	1.2	0.21
$x = 0.6$	$C1(12k)$	0.36	0.41	412	43.5	0.37
	$C2(4f_2)$	0.39	0.17	512	11.5	0.25
	$C3(4f_1)$	0.27	0.21	485	24.1	0.40
	$C4(2a)$	0.38	0.09	500	7.5	0.28
	$C5(2b)$	0.28	2.22	396	4.2	0.30
	$C6(12k^1)$	0.33	0.35	353	7.8	0.47
	$C7(4f_2^1)$	0.73	−0.44	427	1.3	0.21
$x = 0.9$	$C1(12k)$	0.36	0.40	411	41.1	0.37
	$C2(4f_2)$	0.39	0.17	510	10.5	0.25
	$C3(4f_1)$	0.27	0.21	483	26.3	0.45
	$C4(2a)$	0.38	0.10	499	6.9	0.27
	$C5(2b)$	0.27	2.20	394	3.8	0.31
	$C6(12k^1)$	0.32	0.36	352	9.8	0.52
	$C7(4f_2^1)$	0.75	−0.44	428	1.6	0.21
$x = 1.2$	$C1(12k)$	0.36	0.40	411	41.9	0.41
	$C2(4f_2)$	0.36	0.16	508	13.1	0.2
	$C3(4f_1)$	0.28	0.21	482	26.9	0.47
	$C4(2a)$	0.39	0.10	496	3.5	0.22
	$C5(2b)$	0.28	2.21	394	3.7	0.31
	$C6(12k^1)$	0.33	0.35	352	9.4	0.49
	$C7(4f_2^1)$	0.73	−0.45	429	1.4	0.21

of Ti^{4+}, by 22.4% at $x = 1.2$ and substitutions with In^{3+}, by 21.9% with Sc^{3+}, and by 6.6% at $x = 1.0$ with Zn^{2+}. This is not completely correlated with ion radii of listed ions of the impurity, suggesting that the degree of substitution is affected by not only ion radii, but electron configuration of the substitution ions as well.

To substantiate the spectra break down of the BaM-Zr hexaferrite by comparing maximum integral intensities of additional sextets with intensities of main positions, these intensities were plotted for $C6(12k^1)$ and $C7(4f_2^1)$ sextets and shown in Fig. 4.

The sum of sextets 1 and C6 over all compositions has shown that within the limits of break-down error and determination of sextet intensities we have a value close to the initial intensity for non-substituted hexaferrite. As for the C7 sextet formed due to the break of $Fe(4f_2){-}O{-}Zr(12k)$

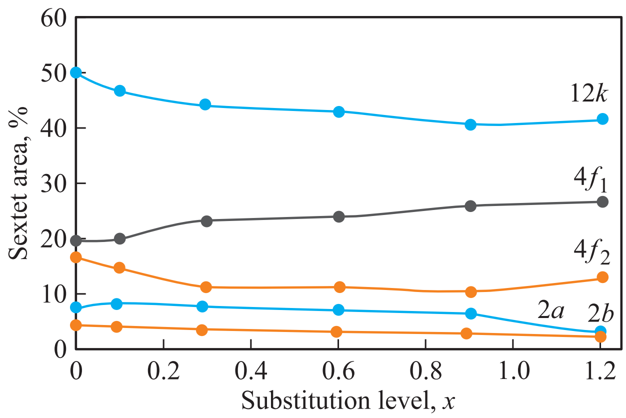

Figure 3. Integral intensities of sextets in spectra of BaM-Zr hexaferrite as functions of the degree of substitution x.

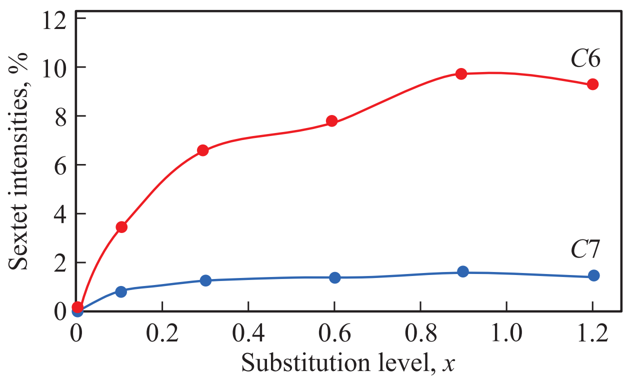

Figure 4. Integral intensities of C6 and C7 sextets in spectra of BaM-Zr hexaferrite as functions of the degree of substitution x.

magnetic bond, the sum of integral intensities of C2 and C7 sextets does not provide for the initial value of 16.8%rel.

It can be seen from the table that for the specimen with $x = 0.1$ (Fig. 2, b) of spectrum C1 the changes are associated mainly with areas of sextets C1 and C2 of positions $12k$ and $4f_2$. A decrease in area of the C1 sextet means entering of Zr^{4+} ions into the $12k$ position. This results in two broken $Fe(12k)-O-Fe(12k)$ bonds in the triad of these octahedrons and formation of two magnetically equivalent positions of Fe^{3+} ions noted as $12k_1$ (C6 sextet). Significant changes in the cation distribution of Zr^{4+} ions took place at $x = 0.3$, consisting in an abrupt decrease in the intensity of the C2 sextet from ions of $Fe(4f_2)$, as well as in increase in the intensity of the C7 sextet from ions of Fe^{2+} and the C3 sextet from ions of $Fe(4f_1)$. The decrease in area of the C2 sextet from ions of $Fe(4f_2)$ is explained by entering of Zr^{4+} ions in this position and the broken $Fe(4f_2)-O-Fe(12k)$ bond with emergence of non-equivalent position of ion $4f_2^1$ (the C7 sextet), at the same time, according to the isomer shift, valence of these ions is 2+, that provides electroneutrality of the hexaferrite. However, the portion of bivalent ion (the C7 sextet) does not provide for the general decrease in intensity of the C2 sextet, because the main part of $Fe^{3+}(4f_2^1)$ ions in the form of additional sextet is superimposed on the C3 sextet increasing its intensity and resonance line width due to incomplete coincidence of the sextets. The magnetic field of the portion of superimposed sextet indicates that it could be formed due to the C2 sextet from $Fe^{3+}(4f_2^1)$ or the C4 sextet from $Fe^{3+}(2a)$, however, the $2a$ sextet intensity remained unchanged, therefore the increase in intensity of the C3 sextet can be explained only by the superimposition of part of the additional C2 sextet from $Fe(4f_2)$. At the same time, the lower magnetic field on nuclei of Fe^{57} ions of iron in the C7 sextet is explained by their bivalent condition. These changes are also continued with increase in x up to 0.6 and further, up to 1.2. The isomer shift and quadrupolar splitting of all sextets at x from 0.1 to 1.2 are in agreement with valence state of iron ions and their coordination.

The observed changes in cation distribution should be reflected on magnetic characteristics of the BaM-Zr hexaferrite as well.

It can be seen from Fig. 5 that all specimens under examination remain in the state of magnetic saturation in external magnetic fields up to 2 T. With increase in the degree of substitution by zinc ions the main magnetic characteristics change in a non-linear manner. For more detailed understanding of the change in magnetic properties for different chemical compositions, Fig. 6 shows the obtained dependencies of specific magnetization and residual magnetization, coercitive force, and squareness ratio .

The specific magnetization of BaM-Zr hexaferrite (Fig. 6, a) as a function of the degree of substitution changes non-monotonously and has a peak at $x = 0.3$ with further decrease to $x = 1.2$. This is compliant with the data of Messbauer spectroscopy that detects the cation redistribution taking place at $x = 0.3$. Since magnetic moments in hexaferrites from $12k$, $2a$, and $2b$ ions are oriented into the same direction, and those of $4f_1$ and $4f_2$ are directed opposite to them, the resulted magnetic moment according to the Neel model is equal to their difference. This results in a decrease in occupation of the $4f_2$ position by Zr^{4+} ions, a rise in magnetization, and further increase in occupation of the $12k$ position decreases it.

The residual magnetization (Fig. 6, b) also reacts on the cation redistribution, and at $x = 0.3$ it has, in contrast to the specific magnetization, a dip with further decrease, which indicates a relationship between these parameters.

The coercitive force (Fig. 6, c) in the range of 0.1–0.3 does not change, and then demonstrates a monotone increases due to the increase in magnetocrystalline anisotropy. Its maximum values do not exceed 2.4 kOe, which is an evidence of low magnetic hardness of the BaM-Zr hexaferrite and its suitability for the use in magnetic amplifiers, cores of transformers and inductors.

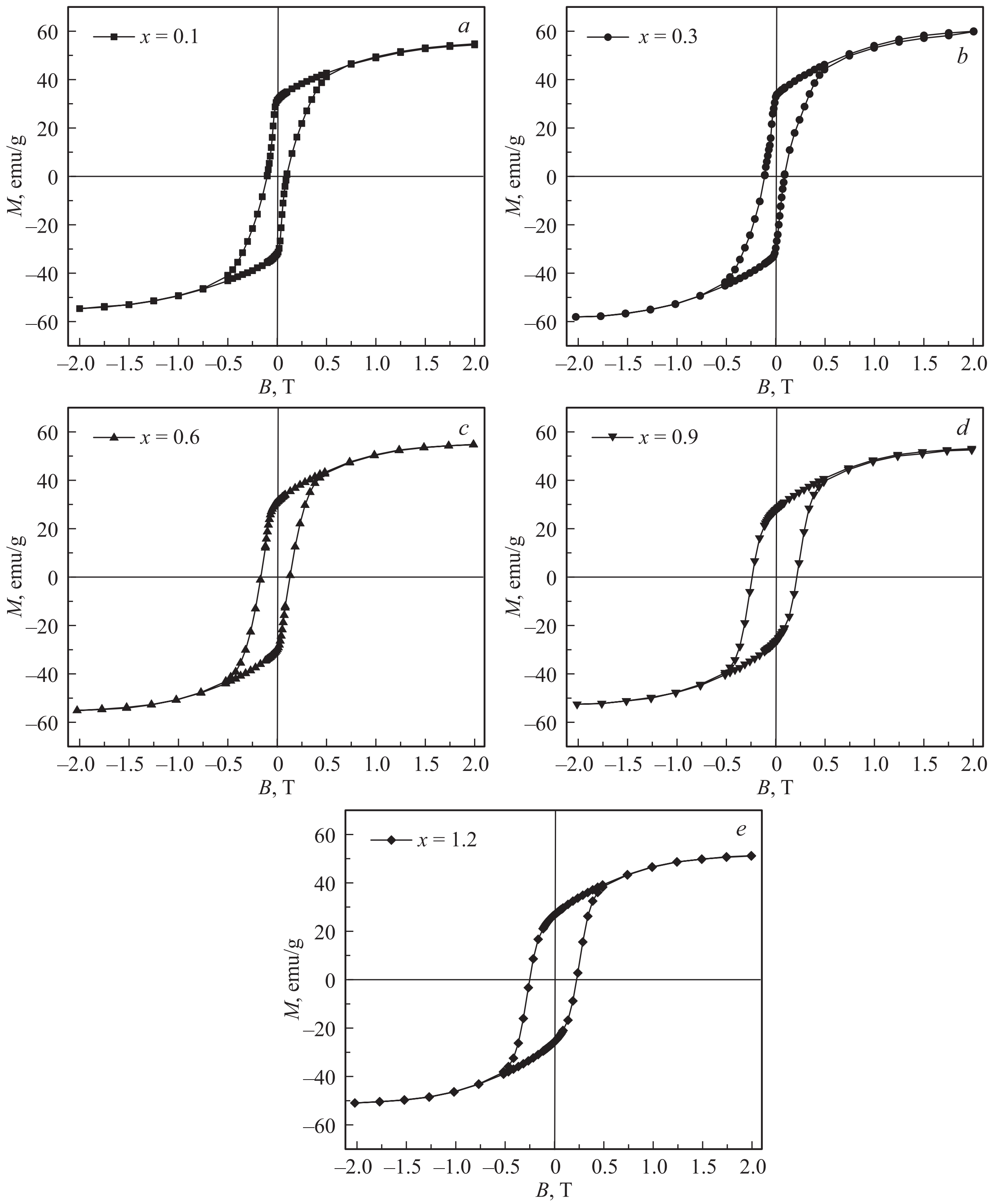

Figure 5. Field dependencies of specific magnetization of BaM-Zr barium hexaferrite specimens.

The Mr/Ms squareness ratio of the hysteresis loop varies in the process of increase in the degree of substitution, and at $x = 1.2$ it demonstrates a low value of 0.51, which restricts the opportunities of hexaferrite use in switching devices of magnetoelectronics.

4. Conclusion

As a result of the performed studies of $BaZr_xFe_{12-x}O_{19}$ barium hexaferrite, it was shown that a limited heterovalent isomorphism takes place in its structure according to the

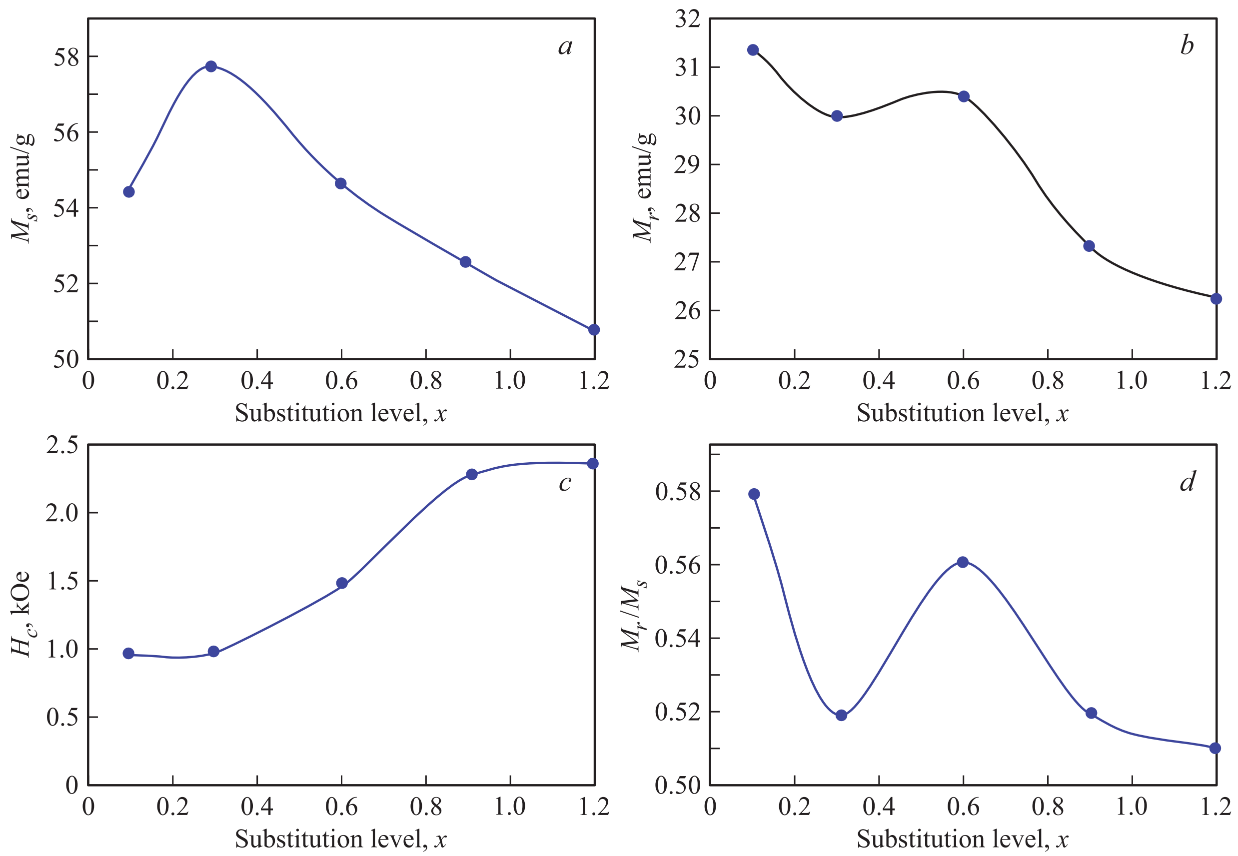

Figure 6. Magnetic characteristics of BaM-Zr hexaferrite: a — saturation magnetization: b — residual magnetization, c — coercitive force, d — Sq = Mr/Ms.

scheme of $2Fe^{3+} \rightarrow Zr^{4+} + Fe^{2+}$. In this case bivalent iron in the structure is diagnosed by the isomer shift of Fe ions in the Messbauer spectra of the hexaferrite. It is found that the limit of the heterovalent isomorphic substitution in the hexaferrite is $x = 0.6$, with zirconium as an independent phase starting manifestation in the form of ZrO_2, which is detected by stationary X-ray diffraction technique, and in the range of $x = 0.6-0.9$, according to the data of Messbauer spectroscopy, partial entering of Zr into the hexaferrite lattice continues. Additional sextets in Messbauer spectra of the barium hexaferrite may be formed with localization of Zr^{4+} ions mainly in $12k$ and $4f_2$ positions due to two broken exchange bonds: $Fe(12k)-O-Fe(12k)$ and $Fe(4f_2)-O-Fe(12k)$, noted as $12k_1$ and $4f_2^1$. The dependence of specific magnetization of BaM-Zr has shown that it has a peak at $x = 0.3$ due to predominance of the $4f_2$ position in this substitution, which is followed by monotone decrease in magnetization with increase in x. The coercitive force in the range of $0.1-0.3$ does not change, and then demonstrates a monotone increases due to the increase in magnetocrystalline anisotropy. Its maximum values are not more than 2.4 kOe, which indicates low magnetic hardness of the BaM-Zr hexaferrite. The performed studies show the limits for the use of the zirconium-doped barium hexaferrite, as well as the possibility to produce specimens with predefined magnetic properties for industrial use.

Funding

This research work was financially supported by the Russian Science Foundation (Agreement No. 19-19-00694 dated 06.05.2019).

Conflict of interest

The authors declare that they have no conflict of interest.

References

[1] A.L. Kozlovskiy, I.E. Kenzhina, M.V. Zdorovets. Cer. Inter. **46**, *8*, 10262 (2020).
[2] M.V. Zdorovets, A.L. Kozlovskiy. J. Alloys Comnd. **815**, 152450 (2020).
[3] A.L. Kozlovskiy, M.V. Zdorovets. Comp. B **191**, 107968 (2020).
[4] Y. Yang, F. Wang, J. Shao, D. Huang, H. He, A.V. Trukhanov, S.V. Trukhanov. J. Alloys Comnd. **765**, 616 (2018).
[5] A.V. Trukhanov, K.A. Astapovich, M. Almessiere, V.A. Turchenko, E.L. Trukhanova, V.V. Korovushkin, A.A. Amirov,

M.A. Darwish, D.V. Karpinsky, D.A. Vinnik, D.S. Klygach, M.G. Vakhitov, M.V. Zdorovets, A.L. Kozlovskiy, S.V. Trukhanov. J. Alloys Comnd. **822**, 153575 (2020).
[6] D.S. Klygach, M.G. Vakhitova, D.A. Vinnik, A.V. Bezborodov, S.A. Gudkova, V.E. Zhivulin, D.A. Zherebtsov, C.P. SakthiDharana, S.V. Trukhanov, A.V. Trukhanov, A.Yu. Starikov. J. Magn. Magn. Matter. **456**, 290 (2018).
[7] D.A. Vinnik, V.E. Zhivulin, A.Yu. Starikov, S.A. Gudkova, E.A. Trofimov, A.V. Trukhanov, S.V. Trukhanov, V.A. Turchenko, V.V. Matveev, E. Lahderanta, E. Fadeev, T.I. Zubar, M.V. Zdorovets, A.L. Kozlovsky. J. Magn. Magn. Matter. **498**, 166117 (2020).
[8] V. Turchenko, V.G. Kostishyn, S. Trukhanov, F. Damay, F. Porcher, M. Balasoiu, N. Lupu, B. Bozzo, I. Fina, A. Trukhanov, J. Waliszewski, K. Recko, S. Polosan. J. Alloys Comnd. **821**, 153412 (2020).
[9] V.V. Korovushkin, A.V. Trukhanov, V.G. Kostishin, I.M. Isayev, I.V. Shchetinin, N.M. Durov, A.Yu. Mironovich, I.O. Minkova, K.A. Astapovich, Physics of the Solid State **62**, *5*, 789 (2020) (in Russian).
[10] A.V. Trukhanov, V.G. Kostishin, V.V. Korovushkin, L.V. Panina, S.V. Trukhanov, V.A. Turchenko, I.S. Polyakov, R.Kh. Rakhmatullin, G.A. Filatov, T.I. Zubar, V.V. Oleinik, Ye.S. Yakovenko, L.Yu. Matsuy, L.L. Vovchenko, V.L. Launets, Ye.L. Trukhanova, Physics of the Solid State **60**, *9*, 1723 (2018) (in Russian).
[11] V.G. Kostishin, V.V. Korovushkin, I.M. Isayev, A.Yu. Mironovich, S.V. Trukhanov, V.A. Turchenko, K.A. Astapovich, A.V. Trukhanov. Physics of the Solid State **63**, *2*, 229 (2021) (in Russian).
[12] A.V. Trukhanov, S.V. Trukhanov, V.G. Kostishin, L.V. Panina, I.S. Kazakevich, V.A. Turchenko, V.V. Kochervinsky, Physics of the Solid State **59**, *4*, 721 (2017) (in Russian).
[13] A.V. Trukhanov, V.G. Kostishyn, L.V. Panina, V.V. Korovushkin, V.A Turchenko, P. Thakur, A. Thakur, Y. Yang, D.A. Vinnik, E.S. Yakovenko, L.Yu. Macuy, E.L. Trukhanova, S.V. Trukhanov. J. Alloys Comnd. **754**, 247 (2018).
[14] A.V. Trukhanov, V.O. Turchenko, I.A. Bobrikov, S.V. Trukhanov, A.I. Balagurov, I.S. Kazakevich. J. Magn. Magn. Matter. **393**, 253 (2015).
[15] S.V. Trukhanov, A.V. Trukhanov, V.A. Turchenko, V.G. Kostishin, L.V. Panina, I.S. Kazakevich, A.M. Balagurov. J. Magn. Magn. Matter. **417**, 130 (2016).
[16] M.N. Shipko, V.V. Korovushkin, V.G. Kostishyn, N.D. Ursulyak, A.G. Nalogin, E.S. Savtchenko. J. Nano-Electron. Phys. **7**, *4*, 04075 (2015).
[17] V.V. Korovushkin, A.V. Trukhanov, V.G. Kostishin, I.M. Isayev, Physics and technology of nanomaterials and structures. Collection of scientific articles of the IV International Scientific and Practical Conference, Kursk (2017). V. 1. P. 229. (in Russian).
[18] V.V. Korovushkin, A.V. Trukhanov, M.N. Shipko, V.G. Kostishin, I.M. Isayev, A.Yu. Mironovich, S.V. Trukhanov, Journal of Inorganic Chemistry **64**, *5*, 463 (2019) (in Russian).
[19] S. Verma, O.P. Pandey, A. Paesano Jr., P. Sharma. Physica B: Condens. Matter. **448**, 57 (2014).
[20] D.A. Vinnik, A.Yu. Tarasova, D.A. Zherebtsov, L.S. Mashkovtseva, S.A. Gudkova, S. Nemrava, A.K. Yakushechkina, A.S. Semisalova, L.I. Isaenko, R. Niewa. Cer. Inter. **41**, 9172 (2015).
[21] T. Tsutaoka, A. Tsurunaga, N. Koga. J. Magn. Magn. Mater. **399**, 64 (2016).
[22] S. Kanagesan, M. Hashim, S. Jesurani, T. Kalavani, I. Ismail. J. Supercond. Nov. Magn. **27**, 811 (2014).
[23] M. Sharma, S.C. Kashyap, H.C. Gupta. Physica B **448**, 24 (2014).
[24] H. Sozeri, Z. Mehmedi, H. Kavas, A. Baykal. Cer. Int., **41**, *8*, 9602 (2015)
[25] V.V. Korovushkin, A.V. Trukhanov, V.G. Kostishin, I.M. Isayev, S.V. Trukhanov, K.A. Astapovich, A.Yu. Mironovich, Inorganic Materials **56**, *7*, 746 (2020) (in Russian).
[26] V.V. Korovushkin, M.N. Shipko, V.G. Kostishin, I.M. Isayev, A.Yu. Mironovich, S.V. Trukhanov, A.V. Trukhanov, Inorganic Materials **55**, *10*, 1065 (2019) (in Russian).